Transport behaviors in graphene field effect transistors on boron nitride substrate

A. Alarcón, V. Hung Nguyen, S. Berrada, D. Querlioz, J. Saint-Martin, A. Bournel and P. Dollfus

Institute of Fundamental Electronics, CNRS, Univ. Paris-Sud, UMR8622, Orsay, France

alfonso.alarcon@u-psud.fr

Abstract - **We model the transport behavior of a top-gated graphene field-effect transistor where boron nitride is used as substrate and gate insulator material. Our simulation model is based on the non-equilibrium Green's function approach to solving a tight-binding Hamiltonian for graphene, self-consistently coupled with Poisson's equation. The analysis emphasizes the effects of the chiral character of carriers in graphene in the different transport regimes including Klein and band-to-band tunneling processes. We predict the possible emergence of negative differential conductance and investigate its dependence on the temperature and the BN-induced bandgap. Short-channel effects are evaluated from the analysis of transfer characteristics as a function of gate length and gate insulator thickness. They manifest through the shift of the Dirac point and the appearance of current oscillations at short gate length.**

Keywords- Graphene field-effect transistor, boron nitride, non-equilibrium Green's functions, short-channel effect, Dirac point

I. INTRODUCTION

The isolation of one-atom-thick layer of graphene triggered a revolution in solid-state physics and gave rise to a lot of expectations towards electronic applications [1,2]. However, the benefits of the extraordinary intrinsic transport properties of graphene [3] are usually hindered by the defects of the supporting insulating substrate. Recently, it has been shown that graphene reported on hexagonal boron nitride (h-BN) has higher mobility than on any other substrate [4]. Indeed, such a substrate is flat, with a low density of charged impurities, does not have dangling bonds and is relatively inert. A mobility of 275 000 cm^2/Vs, as high as for suspended graphene, has even been reported [5]. It should allow reaching ballistic transport even at room temperature and exploiting the peculiarities of graphene properties inherent in the massless and chiral character of charge carriers, which may manifest through chiral band-to-band and Klein tunneling [6]. Additionally, h-BN has the same atomic structure as graphene, with a lattice constant 1.8% higher. It offers the possibility of assembling graphene/BN multilayers. In the case of Bernal stacking, it has been shown that the interaction of BN with graphene may open a bandgap of 53 meV [7] or even 100 meV [8] in graphene, which could improve the poor pinch-off characteristic of graphene field-effect transistors (GFETs).

In this work, we investigate the device operation and electrical characteristics of GFETs for different gate lengths (between 10 nm and 100 nm) and gate insulator thicknesses (2 nm, and 10 nm), including the possibility of a BN-induced bandgap opening (53 meV and 100 meV).

II. DEVICE TRANSPORT MODEL

In Fig. 1(a) we display the schematic view of the simulated top-gated GFET wherein the channel is formed by a monolayer graphene sheet in the Oxy plane. The source and drain extensions are N-type doped to 10^{13} cm^{-2}. All other simulation parameters are given in the figure captions. We assume the lateral width of the device to be much larger than the channel length, so that the y direction can be considered through Bloch periodic boundary conditions [9,10].

Now, we summarize the most important features of the transport model used to compute the current density. In this model, the Hamiltonian of the graphene channel is considered via a nearest-neighbor tight-binding approximation [11], i.e.

$$H_{tb} = \sum_n \varepsilon_n |n\rangle\langle n| - t \sum_{\langle n,m\rangle} \left[|n\rangle\langle m| + |m\rangle\langle n| \right], \quad (1)$$

where n and m refer to the nearest atomic sites of the 2D lattice, ε_n is the on-site energy and $t = 2.7$ eV is the next-neighbor hopping energy [12]. The Schrödinger equation is solved within the non-equilibrium Green's function (NEGF) formalism. In the ballistic approximation the retarded Green's function writes

$$G^r(E) = \left[\left(E - i0^+\right)I - H_{tb} - \Sigma_S - \Sigma_D \right]^{-1}, \quad (2)$$

where E is the charge energy of the system and the self energies $\Sigma_{S,D}$ describe the coupling between the graphene channel and the semi-infinite contacts. Then, the charge density in the channel is computed as

$$\rho(x) = \frac{1}{\pi} \int_{-\infty}^{\infty} dE \int_{BZ} dk_y$$
$$\times \left\{ D_S(E,x) \left[f_S(E) + \left(\mathrm{sgn}(E - E_N) - 1\right)/2 \right] \right., \quad (3)$$
$$\left. + D_D(E,x) \left[f_D(E) + \left(\mathrm{sgn}(E - E_N) - 1\right)/2 \right] \right\}$$
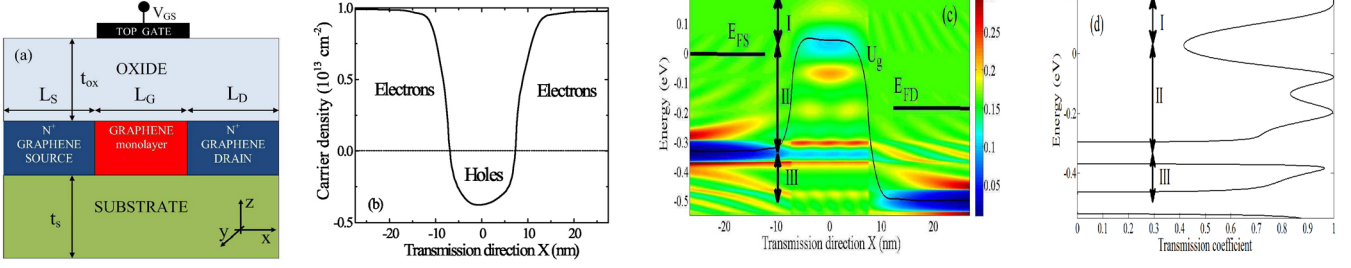
Figure 1. (a) Scheme of the simulated GFET. H-BN is used as substrate and oxide material with a dielectric constant $\varepsilon_r = 3.5$. (b) Local carrier density (negative values correspond to holes). The horizontal dashed line is a guide to the eye. (c) Potential profile (solid line) and LDOS for the transverse momentum $k_y = K_y + 6.4 \times 10^7$ m^{-1}. E_{FS} and E_{FD} are the Fermi levels in source and drain contacts, respectively. (d) Corresponding transmission coefficient as a function of the energy. Device parameters for (b), (c) and (d): $N_D = 10^{13}$ cm^{-2}, $L_{S,D} = L_G = 20$ nm, $t_{ox} = 2$ nm, $t_S = 100$ nm, $V_{DS} = 0.2$ V, $V_{GS} = - 0.5$ V, $E_{GAP} = 0$ meV, and $T = 300$ K.

where E_N is the charge neutrality level, sgn(E) is the sign function, $f_{S(D)}$ are the source and drain Fermi distributions with the Fermi levels $E_{FS(FD)}$ respectively, $D_{S(D)} = G\Gamma_{S(D)}G^\dagger$ is the local density of states (LDOS) resulting from the source(drain) states, and $\Gamma_{S(D)} = i\left(\Sigma_{S(D)} - \Sigma^\dagger_{S(D)}\right)$ is the injection rate at source(drain) contact. The NEGF transport equations are solved self-consistently with the Poisson equation. The method of moments [13], known to be computationally efficient, is used to solve this equation. Since the potential is assumed to be y-independent, the Poisson equation is solved in the 2D-space Oxz. The self-consistence is implemented through the Newton-Raphson method [14]. The updated values of potential U_g are introduced as on-site energies ε_n in (1). The whole process is repeated until the convergence is reached. Finally, the current density is computed as

$$J = \frac{q}{\pi h}\int_{-\infty}^{\infty} dE \int_{BZ} dk_y\, T(E, k_y)\left[f_s(E) - f_D(E)\right], \quad (4)$$

where $T(E, k_y) = \text{Trace}\left[\Gamma_S G \Gamma_D G^\dagger\right]$ is the transmission function. A more detailed discussion on the full algorithm used can be found in [15].

III. NUMERICAL RESULTS

In Fig. 1(b) and Fig. 1(c), we present the self-consistent result of the carrier density and the potential profile U_g, respectively, for $V_{GS} = -0.5$ V and $V_{DS} = 0.2$ V. The corresponding transmission coefficient is displayed in Fig. 1(d). The chirality of carriers appears in the density profile of Fig. 1(b) which exhibits positive (electrons) and negative (holes) values outside and inside the gated region, respectively. In Fig. 1(c) the local density of states (LDOS) is also plotted for a transversal momentum $k_y = (2/3 + 0.005)\pi/a_c\sqrt{3}$ where $a_c = 0.142$ nm is the lattice constant. Though the graphene bandgap is actually zero, we observe in Fig. 1(c) an apparent energy gap in the plot of LDOS. This feature can be explained

in terms of energy band structure of graphene which gives rise to a k_y-dependent energy gap which writes [16]

$$\hat{E}_g = 2t\left|1 - 2\cos\left(a_c k_y \sqrt{3}/2\right)\right|. \quad (5)$$

This energy gap is truly zero for $k_y = K_y = 2\pi/3a_c\sqrt{3}$ (transversal momentum at Dirac Point) but finite for $k_y \neq K_y$. For instance, $\hat{E}_g(k_y) \approx 77$ meV for $k_y = K_y + 6.4 \times 10^7$ m^{-1}, as seen in Fig. 1(c). This energy gap plays an important role since it governs the off current and the negative differential conductance (NDC) effect which will be discussed later.

Observing both the LDOS and the transmission coefficient is useful to understand well the different transport regimes and their connection with the chiral character of carriers. We can separate these transport regimes in energy regions (I), (II) and (III), as schematized in Figs. 1(c) and (d). The first is the thermionic regime (I) for energies above the potential barrier. The second is the chiral tunneling regime (II) that results from the good matching of the hole states in the gated region with the electron states in the source [17,18]. It appears clearly in Fig. 1(d) where the transmission coefficient exhibits resonant peaks in the energy range [-0.3,0]. The transport regime (III) corresponds to the chiral band-to-band tunneling between hole states in the source and electron states in the drain. We will see in this work that because of the zero (or small) bandgap, these transport regimes play an important role in the electrical characteristics. For example, we measure now the contribution of the different transmission regimes in the current-voltage characteristics plotted in Fig. 2 for the gate length $L_G = 15$ nm and for three values of V_{GS}. The total current density (black line) is the sum of the three contributions (I), (II), and (III). for $V_{GS} = - 0.5$ V (Fig. 2(a)) the chiral tunneling is the dominant process at low drain bias but reduces at high V_{DS} where the band-to-band and the thermionic regimes increase monotonically, which makes the saturation of current impossible. For $V_{GS} = 0$ V (Fig. 2(b)) the chiral and the thermionic currents are dominant and comparable at low drain bias. When increasing the drain bias the most important contributions become the thermionic current and, on a smaller extent, the band-to-band transmission (at very high bias).
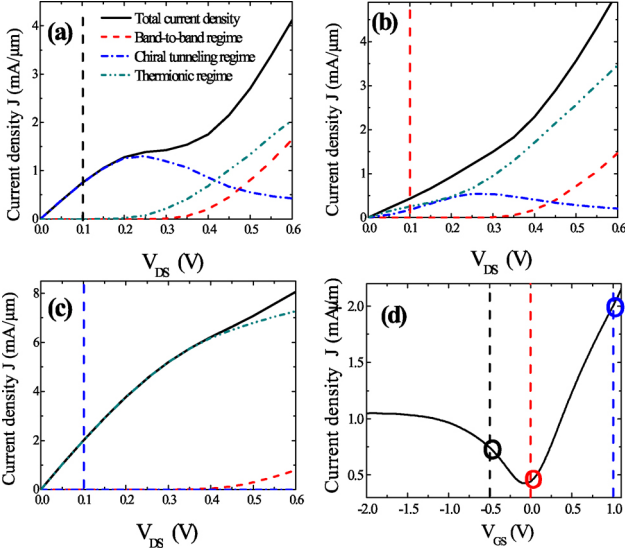
Figure 2. Current-voltage characteristics for different values of V_{GS}: (a) $V_{GS} = -0.5$ V (b) $V_{GS} = 0$ V and (c) $V_{GS} = 1$ V. In (d) We show in the vertical dashed lines the corresponding V_{GS} values in the transfer characteristic for $V_{DS} = 0.1$ V. Device parameters: $N_D = 10^{13}$ cm^{-2}, $L_{S,D} = 20$ nm, $L_G = 15$ nm, $t_{ox} = 2$ nm, $t_s = 100$ nm, $E_{GAP} = 0$ meV, and $T = 300$ K.

Finally, in Fig. 2(c) it is clear that for $V_{GS} = 1$ V the thermionic regime is the strongly dominant transport regime, with a small contribution of the band-to-band tunneling at very high drain voltage. The vertical dashed lines in Figs. 2(a), (b) and (c) correspond to the three values of V_{GS} marked with vertical dashed lines in the transfer characteristic of Fig. 2(d).

In Fig. 3, we present the current-voltage characteristics for different values of V_{GS}. At high V_{DS} a rapid and quasi-linear increase of the current density is observed in almost all cases. This feature is essentially due to the contribution of thermionic transport. At lower V_{DS} we see a weak saturation behavior and in some cases an NDC effect. The NDC arises when the k_y-transmission energy gap at the top of the barrier enters the window [E_{FS} - E_{FD}][18,19]. It is observed at low V_{GS} and for the very thin insulator layer $t_{ox} = 2$ nm. It tends to be washed out when increasing t_{ox} (not shown) and the temperature (as commented below). The general behavior presented in Fig. 3 is consistent with the experimental results of [20]. In Fig. 4 is plotted the current-voltage characteristics of a 50 nm gate length device as a function of the drain bias V_{DS} for the E_{GAP} values of 0 meV, 53 meV and 100 meV [7,8], and for the temperatures $T = 77$ K and $T = 300$ K. The NDC effect appears to be strongly dependent on the value of the BN-induced bandgap in graphene and by the value of temperature. The peak-to-valley ratio (PVR) can reach ≈ 3 for $E_{GAP} = 100$ meV at $T = 77$ K.

In Fig. 5 we show the transfer characteristic for different gate lengths L_G. At short gate length, we observe an oscillation of current for negative values of V_{GS}.
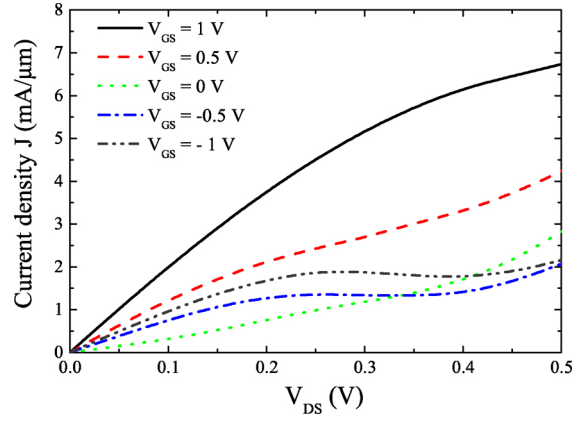

Figure 3. Current-voltage characteristics for different values of V_{GS}. Device parameters: $N_D = 10^{13}$ cm^{-2}, $L_G = 50$ nm, $L_{S,D} = 20$ nm, $t_{ox} = 2$ nm, $t_s = 100$ nm, $E_{GAP} = 0$ meV, and $T = 300$ K
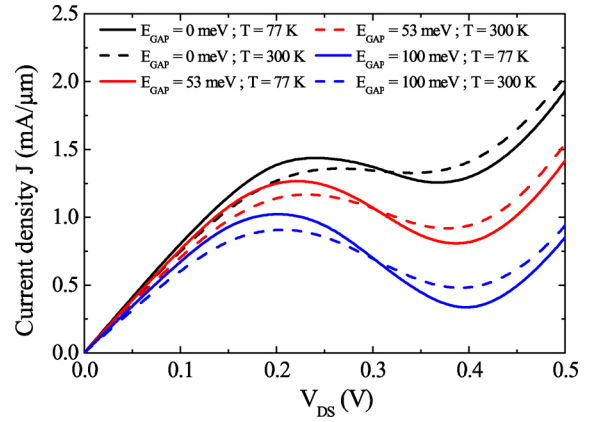

Figure 4. Current-voltage characteristics for different bandgap values and for different values of temperature: $T = 77$ K and $T = 300$ K. Device and simulation parameters: $N_D = 10^{13}$ cm^{-2}, $L_G = 50$ nm, $L_{S,D} = 20$ nm, $t_{ox} = 2$ nm, $t_s = 100$ nm, and $V_{GS} = -0.5$ V.
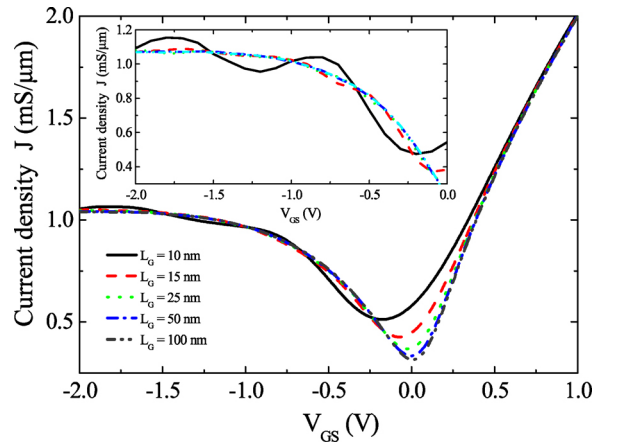

Figure 5. Transfer characteristics for different gate lengths. Device parameters: $L_{S,D} = 20$ nm, $t_{ox} = 2$ nm, $t_s = 100$ nm, $V_{DS} = 0.1$ V, $E_{GAP} = 0$ meV, and $T = 300$ K. In the inset, the same device parameters except $T = 77$ K.
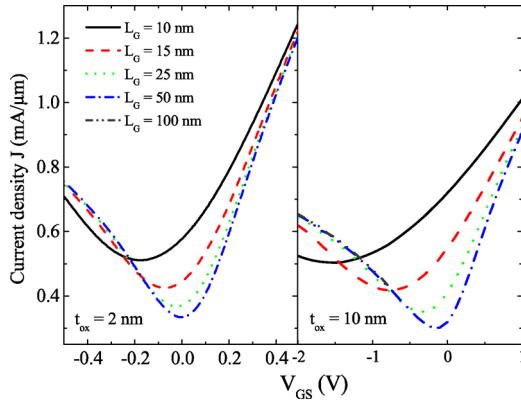
Figure 6. Zoom of the Fig. 5 around the Dirac points in transfer characteristics for different L_G (a) $t_{ox} = 2$ nm. (b) $t_{ox} = 10$ nm. Device parameters: $V_{DS} = 0.1$ V, $E_{GAP} = 0$, $t_s = 100$ nm, and $T = 300$ K.

As we show in the inset of Fig. 5 this oscillation increases when decreasing the temperature. The oscillation results from the quantization of hole states in the gated region which gives rise to resonant chiral tunneling [18]. A zoom of Fig. 5 around the Dirac point is shown in Fig. 6 for two values of the gate insulator thickness: $t_{ox} = 2$ nm and $t_{ox} = 10$ nm. When reducing L_G, a shift of the Dirac point to negative V_{GS} values is observed. This short channel effect is due to the reduced gate charge control at short gate length which makes necessary to apply a more negative V_{GS} value to reach the Dirac point, i.e. the transition between normal transmission above the barrier and chiral tunneling through the barrier. This short channel effect is obviously stronger when increasing t_{ox}. It was experimentally observed in [21].

IV. CONCLUSIONS

We have presented different features of transport behaviour in a top-gated GFET where h-BN was used as both substrate and gate oxide material. This study was performed by means of self-consistent simulation of the 2D-Poisson equation and the non-equilibrium Green's function approach to solving a tight-binding Hamiltonian. The analysis of the different transport regimes provided an understanding of the transport behaviours and emphasized the important role of chiral (Klein and band-to-band) tunnelling processes. An NDC effect has been shown to occur at negative V_{GS} as a consequence of the k_y-transmission energy gap at the top of the barrier. The PVR of NDC is dependent on the bandgap in graphene and on the temperature. It may reach the value of 3 at $T = 77$ K. The gate insulator thickness was shown to strongly influence the short-channel effects through the gate length dependence of the Dirac point position in the transfer characteristics. At very small gate length, the chiral tunneling through quantized hole states of the channel was shown to give rise to current oscillations.

ACKNOWLEDGMENT

REFERENCES

[1] K. S. Novoselov, A. K. Geim, S. V. Morozov, D. Jiang, Y. Zhang, S. V. Dubonos, I. V. Grigorieva, A. A. Firsov, "Electric field effect in atomically thin carbon films," Science, vol. 306, pp. 666-669, Oct. 2004.

[2] M. C. Lemme, T. J. Echtermeyer, M. Baus, H. Kurz, "A Graphene field-effect device, " IEEE Electron Device Lett., vol. 28, pp. 282-284, Apr. 2007.

[3] K. I. Bolotin, K. J. Sikes, Z. Jiang, M. Klima, G. Fudenberg, J. Hone, P. Kim, H. L. Stormer, "Ultrahigh electron mobility in suspended graphene," Solid State Commun., vol. 146, pp. 351-355, May. 2008.

[4] C. R. Dean, A. F. Young, I. Meric, C. Lee, L. Wang, S. Sorgenfrei, K. Watanabe, T. Taniguchi, P. Kim, K. L. Shepard and J. Hone, "Boron nitride substrates for high-quality graphene electronics," Nature Nanotechnol., vol. 5, pp. 722-726, Aug. 2010.

[5] P. J. Zomer, S. P. Dash, N. Tombros, and B. J. van Wees, "A transfer technique for high mobility graphene devices on commercially available hexagonal boron nitride," Appl. Phys. Lett., vol. 99, p. 232104, Dec. 2011.

[6] M. I. Katsnelson, K. S. Novoselov, and A. K. Geim, "Chiral tunneling and the Klein paradox in graphene," Nature Phys., vol. 2, pp. 620-625, Aug. 2006.

[7] G. Giovannetti, P. A. Khomyakov, G. Brocks, P. J. Kelly, and J. van den Brink, "Substrate-induced band gap in graphene on hexagonal boron nitride: Ab initio density functional calculations," Phys. Rev. B., vol. 76, p. 073103, Aug. 2007.

[8] N. Kharche and S. K. Nayak, "Quasiparticle band gap engineering of graphene and graphone on Hexagonal Boron nitride substrate," Nano Lett., vol. 11, pp. 5274 - 5278, Oct. 2011.

[9] G. Fiori, G. Iannaccone, "On the possibility of tunable-gap bilayer graphene FET," IEEE Electron Device Lett., vol. 30, pp. 261-264, Mar. 2009.

[10] V. Hung Nguyen, F. Mazzamuto, J. Saint-Martin, A. Bournel, P. Dollfus, "Graphene nanomesh-based devices exhibiting a strong negative differential conductance effect," Nanotechnology, vol. 23, p. 065201, 2012.

[11] V. Hung Nguyen, V. Nam Do, A. Bournel, V. Lien Nguyen, and P. Dollfus, "Controllable spin-dependent transport in armchair graphene nanoribbon structures," J. Appl. Phys., vol. 106, p. 053710, Sep. 2009.

[12] S. Reich, J. Maultzsch, and C. Thomsen "Tight-binding description of graphene," Phys. Rev. B, vol. 66, p. 035412, Jul. 2002.

[13] J. Guo, S. Datta, M. P. Anantram, and M. Lundstrom, "Atomistic simulation of carbon nanotube field-effect transistors using non-equilibrium green's function formalism," J. Comput. Electron., vol. 3, pp. 373-377, Oct. 2004.

[14] Z. Ren, "Nanoscale MOSFETs: Physics, Simulation, and Design," PhD. Thesis, Purdue University, West Lafayette, 2001.

[15] V. Hung Nguyen, "Electronic transport and spin effects in graphene nanostructures," PhD. Thesis, University of Paris-Sud, France, 2010.

[16] A. H. Castro Neto, F. Guinea, N. M. R. Peres, K. S. Novoselov and A. K. Geim, "The electronic properties of graphene," Rev. Mod. Phys., vol. 81, pp. 109 - 162, Feb. 2009.

[17] V. Hung Nguyen, A. Bournel, C. Chassat, and P. Dollfus, "Quantum transport of Dirac fermions in graphene field effect transistors", in Proc. SISPAD, pp. 9-12, Sep. 2010.

[18] V. Nam Do, V. Hung Nguyen, P. Dollfus, and A. Bournel, "Electronic transport and Spin-polarization effects of relativistics like particles in mesoscopics graphene structures," J. Appl. Phys., vol. 104, p. 063708. Sep. 2008.

[19] Y. Wu, D. B. Farmer, W. Zhu, S.J. Han, C. D. Dimitrakopoulos, A. A. Bol, P. Avouris, and Y. M. Lin, "Three-Terminal Graphene Negative Differential Resistance Devices", ACS Nano, vol. 6 (3), pp 2610–2616 Feb. 2012.

[20] I. Meric, M. Y. Han, A. F. Young, B. Ozyilmaz, P. Kim, and K. L. Shepard, "Current saturation in zero-bandgap, top-gated graphene field-effect transistors", Nature Nanotechnology, vol. 3, pp. 654 - 659 2008.

[21] S. J. Han, Z. Chen, A. A. Bol, and Y. Sun, "Channel-length-dependent transport behaviors of Graphene field-effect transistors", IEEE Electron Device Lett. vol. 32, pp 812-814 June 2011.